ADVANCED SCIENCE NEWS
www.advancedsciencenews.com



# Self-Expansion Construction of Ultralight Carbon Nanotube Aerogels with a 3D and Hierarchical Cellular Structure

*Yufeng Luo, Shu Luo, Hengcai Wu, Mengya Li, Ke Wang, Lingjia Yan, Kaili Jiang,* Qunqing Li, Shoushan Fan, and Jiaping Wang**

***A** novel and simple strategy is developed to construct ultralight and 3D pure carbon nanotube (CNT) aerogels by the spontaneous expansion of superaligned CNT films soaked in a piranha (mixed $H_2SO_4$ and $H_2O_2$) solution, followed by cryodesiccation. The macroscopic CNT aerogels have an extremely low apparent density (0.12 mg $cm^{-3}$), ultrahigh porosity (99.95%), high specific surface area (298 $m^2$ $g^{-1}$), and a hierarchical cellular structure with giant and ultrathin CNT sheets as cell walls. The pure CNT aerogels show high adsorption abilities for various kinds of solvents, and have great potential in widespread applications such as energy storage, catalysis, and bioengineering.*

## 1. Introduction

Since carbon nanotubes (CNTs) were reported in 1991,[1] they have drawn intensive attention from researchers because of their superior electrical and mechanical properties. Studies on macroscopic architectures of CNTs such as wires,[2] fibers,[3] buckypapers,[4] arrays,[5] and aerogels[6,7] have attracted great interests for applications in energy storage,[8,9] catalysis,[10] oil adsorption,[11] and tissue engineering.[12] CNT aerogels play a vital role in these applications as they are highly porous, lightweight, hydrophobic, chemically stable, and have a 3D structure, high electrical conductivity, and excellent thermal insulating capacity.[13] The three most common types of CNT-based aerogels reported in the literature are CNT-polymer aerogels,[6] CNT-graphene aerogels,[14,15] and pure CNT aerogels.[16,17] Among them, CNT-polymer aerogels have been investigated most extensively because of their simple preparation and compatibility with a wide range of CNTs. Polymer agents serve as the surface coating layer and as binders to join the discrete CNTs in CNT-polymer aerogels. Applications of CNT-polymer aerogels have been very limited owing to a large amount of polymer additive needed, reduced electrical conductivity, and relatively high density ($\rho \geq 10$ mg $cm^{-3}$). Compared with CNT-polymer aerogels, CNT-graphene aerogels possess advantages, such as low density, high electrical conductivity, and excellent chemical and environmental stability.[18–20] The stacking of 2D graphene membranes results in aerogels with a cellular structure and a low density because of the high cell-to-wall ratio.

It is very challenging to fabricate ultralight, pure CNT aerogels at a large scale because it is difficult for CNTs to autoweave into a macroporous cellular structure without the support of a polymer or graphene. Here, we demonstrate a novel and simple strategy to construct 3D, ultralight, pure CNT aerogels by the spontaneous expansion of superaligned CNT (SACNT) films soaked in a piranha solution at room temperature, followed by cryodesiccation. The multifunctional and macroscopic CNT aerogels exhibited a typical hierarchical porous and cellular structure assembled from giant and ultrathin CNT sheets as cell walls, and had a unique multilevel structure that was built from 1D CNTs

Y. F. Luo, Dr. S. Luo, Prof. S. S. Fan
Department of Physics and Tsinghua-Foxconn Nanotechnology Research Center
School of Materials Science and Engineering
Tsinghua University
Beijing 100084, P. R. China
H. C. Wu, M. Y. Li, Dr. K. Wang, L. J. Yan, Prof. K. L. Jiang, Prof. Q. Q. Li, Prof. J. P. Wang
Department of Physics and Tsinghua-Foxconn Nanotechnology Research Center
Tsinghua University
Beijing 100084, P. R. China
E-mail: JiangKL@tsinghua.edu.cn; jpwang@tsinghua.edu.cn

DOI: 10.1002/smll.201700966

that formed 2D CNT sheets, and then 3D CNT aerogels. The pure CNT aerogels possessed an extremely low apparent density (0.12 mg $cm^{-3}$), ultrahigh porosity (99.95%), high specific surface area (298 $m^2$ $g^{-1}$), hydrophobicity, and chemical stability. The pure CNT aerogels showed great potential for the adsorption of organic solvents and oils, with an incredibly high adsorption capacity of 1389 mg $mg^{-1}$ for phenixin, and 912 mg $mg^{-1}$ for vegetable oil, which are the highest values reported in the literature.

## 2. Results and Discussion

### 2.1. Preparation and Dimensional Variations of Pure CNT Aerogel

The preparation of the pure CNT aerogel is illustrated in **Figure 1**. Multiwalled SACNT arrays with a tube diameter of 20–30 nm and a height of 300 µm were synthesized on 4 inch silicon wafers in a low pressure chemical vapor deposition (CVD) system, with iron as the catalyst and acetylene as the precursor. SACNTs possessed large aspect ratio (≈$10^4$), high purity, clean surface, and strong interaction among tubes. SACNT sheet was continuously drawn from SACNT arrays by an end-to-end joining mechanism (Figure 1a, the alignment of SACNTs was parallel to the drawing direction)[21–24] and then rolled into a unidirectional multilayer film with 200 layers (Figure 1b). A piranha solution was prepared by mixing solutions of concentrated 98 wt% $H_2SO_4$ and 35 wt% $H_2O_2$ at a volume ratio of 7:3 in a large quartz sink. The SACNT film was cut into 3 × 3 $cm^2$ pieces (≈3.3 mg) and one piece was placed in the piranha solution. The SACNT film piece floated on the piranha solution and began to self-expand spontaneously, which was accompanied by a continuous release of a large number of bubbles from the interlayers of the swelled SACNT film (Figure 1c, Video 1 (Supporting Information) at 60 times the actual speed). As a consequence, the original 3 × 3 $cm^2$ CNT film turned into a large 3D CNT aerogel after the self-expansion and subsequent cryodesiccation. As illustrated in Figure 1d,

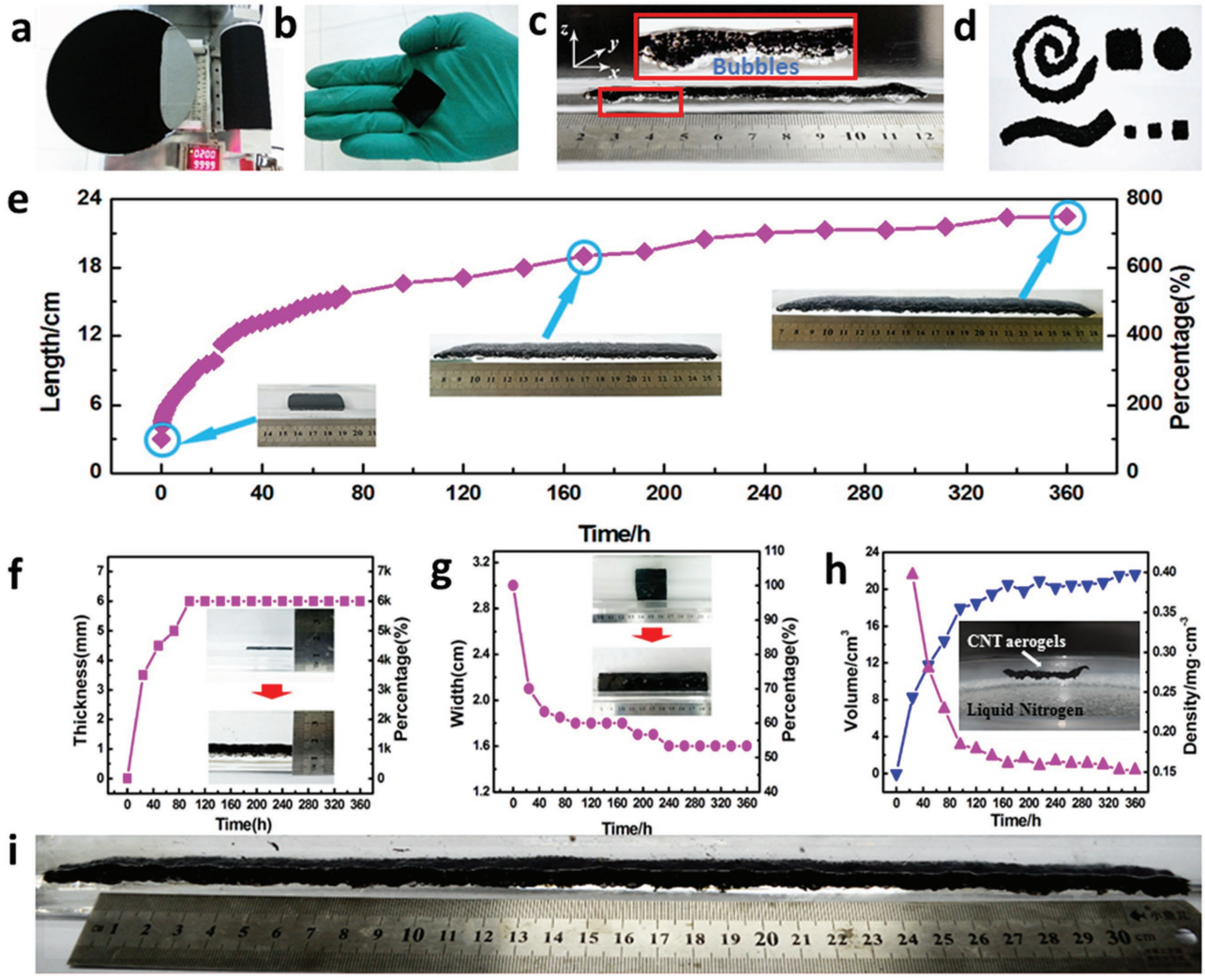


**Figure 1.** a) An SACNT film drawn from an SACNT array on a silicon wafer. b) Photograph of a rolled SACNT film. c) An SACNT film floating on the surface of a piranha solution and generating a large number of bubbles. d) CNT aerogels with various shapes and densities. The dimensional variations of the e) length, f) width, g) thickness, and h) volume and density of the CNT aerogel. i) Photograph of the CNT aerogel after it was immersed in the piranha solution for one month.

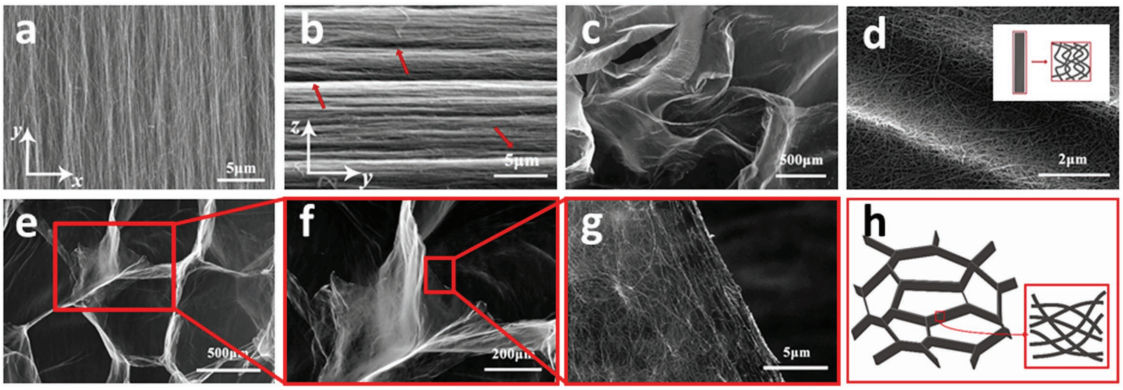


**Figure 2.** Scanning electron microscopy (SEM) images of the a) top surface, b) cross section of the CNT film, and c,d) surface of the CNT aerogel. e) Low-magnification, f) high-magnification, and g) side view SEM images, and h) schematic of the CNT aerogel showing the microstructure of the macropores and CNT sheets.

macroscopic CNT aerogels with tunable sizes and desired shapes, such as spirals, cubes, and cylinders, could be obtained by controlling the size of the original CNT film, immersion time in the piranha solution, and shape of the containers during the cryodesiccation process.

To study the self-expansion process of the SACNT film, the dimensional variations of the length (*x*-axis), width (*y*-axis), and thickness (*z*-axis) were measured. Figure 1e shows the large elongation of the length of the CNT film. The film was stretched to 22.5 cm in 15 d, which was 7.5 times the original length (≈3 cm). The elongation during the first 2 d (≈13.8 cm) was larger than during the subsequent 13 d (≈8.8 cm), demonstrating rapid expansion at the beginning and then a gradual decrease in the expansion rate. Similar variations were observed for the thickness (Figure 1f). The thickness rapidly increased during the first day and reached 0.35 cm, which corresponded to an incredible thickening of 3500 times the original thickness (10 μm). The aerogel continued to swell and was 0.6 cm thick after 15 d. On the contrary, the width of the CNT film reduced from 3 to 1.6 cm after 15 d (Figure 1g). The volume and apparent density of the CNT aerogel were calculated and are shown in Figure 1h. After 15 d, the volume of the CNT aerogel increased to 21.6 $cm^3$, which was 2400 times higher than the original volume of the CNT film; meanwhile, the apparent density of the CNT aerogel changed from the initial 36.67 mg $cm^{-3}$ to the final 0.15 mg $cm^{-3}$. After one month, the CNT aerogel gradually expanded to a size of $36 \times 1.3 \times 0.6$ $cm^3$, which was 3120 times the original size (Figure 1i). Accordingly, the density of the CNT aerogel decreased to as low as 0.12 mg $cm^{-3}$. Notably, this ultralight CNT aerogel is the lightest carbon aerogel ever reported in the literature.[9,10,12–14,16–20] The inset photograph in Figure 1h demonstrates that the CNT aerogel could even float on the cold flow caused by liquid nitrogen underneath, further confirming its ultralight feature.

### 2.2. Microstructure and Morphology of CNT Film and Aerogel

The microstructure and morphology of the CNT film and aerogel were investigated by scanning electron microscopy (SEM). The CNT bundles in the CNT film were closely arranged and parallel to each other, with a denser packing of CNTs in the cross-section (**Figure 2**b, *yz*-plane) than those on the top surface (Figure 2a, *xy*-plane). The piranha solution infiltrated into the CNT film by capillary action; the solution was more likely to permeate and temporarily store in the relatively large gap between the CNT sheets (red arrows in Figure 2b), where macropores in the CNT aerogels could generate by the release of bubbles. Because of the generation of the large pores, the surface of the CNT aerogel became uneven and contained some wrinkles (Figure 2c), and the pristine ordered coaxial CNT bundles became more disordered and curved (Figure 2d). The change from an ordered to a disordered state of the CNT film was further supported by the pole figures of the (002) plane obtained using X-ray diffraction (**Figure 3**), which demonstrated a typical fiber-like texture with good alignment of CNTs in the original CNT film[25] and a disordered state in the CNT aerogel.

The cross-sectional SEM images of the CNT aerogel show a typical macroporous and interconnected cellular structure in which the cells were encircled by giant and ultrathin CNT

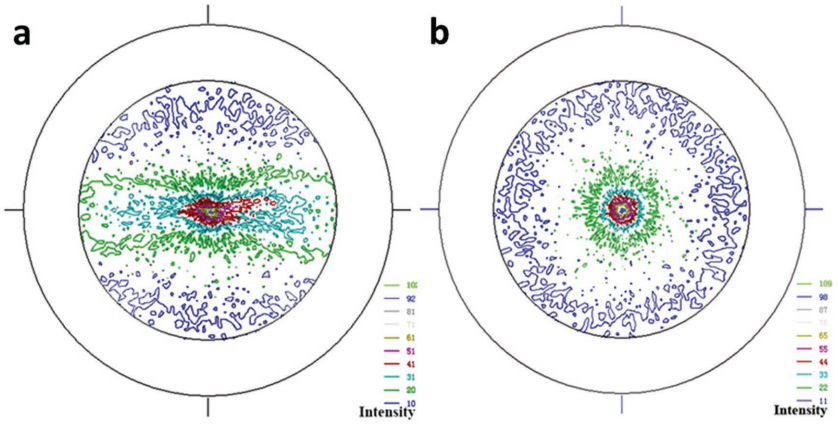


**Figure 3.** Pole figures of a) CNT film and b) CNT aerogel for the (002) plane ($2\theta = 26°$).

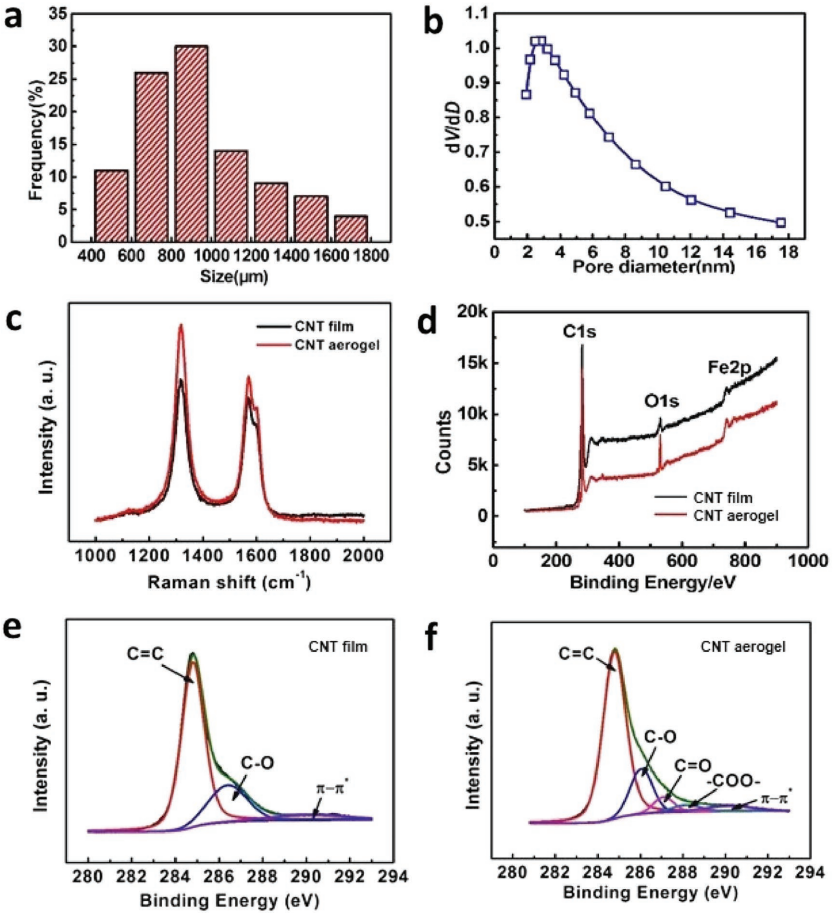


**Figure 4.** a) Histogram of the macropore size and b) pore-size distribution of nanosized pores in the CNT aerogel. c) Raman spectra, d) XPS spectra, and deconvolution of the C1s XPS of e) the CNT film and f) the CNT aerogel.

sheets as the cell walls (Figure 2e and Figure S1, Supporting Information). High-magnification SEM images (Figure 2f,g) indicated that the translucent 2D CNT sheets contained only one or a few layers of a silk-like and highly porous CNT web, formed by interwoven 1D CNT bundles. As shown schematically in Figure 2h, the self-assembled 3D CNT aerogel possessed a multilevel structure of 1D CNTs forming 2D CNT sheets and then a 3D CNT aerogel.

**Figure 4**a shows that the pore of the CNT aerogel ranged from 400 to 1800 μm, with an average size of ≈900 μm and a porosity of more than 99.95%. Additionally, interconnected macropores also provided channels for active materials to flow through and access the inner surfaces of the CNT aerogel. The isothermal adsorption–desorption curves of the CNT aerogel measured by the Brunauer–Emmett–Teller (BET) method showed a typical microporous structure of the cell walls, and demonstrated a high specific surface area of 298 $m^2\ g^{-1}$ (Figure 4b). The specific surface area of a pristine CNT film was only about 180 $m^2\ g^{-1}$ (Figure S2, Supporting Information), which was at the same level with those of multiwalled CNTs reported in the literature[25–29] and almost one magnitude lower than those of single-walled CNT aerogels.[7,30,31] By performing the piranha solution treatment, the CNT aerogel obtained higher specific surface area than the pristine CNT film. Due to the high aspect ratio of CNTs (≈$10^4$), it was difficult for the nitrogen molecules to cover the entire interior surfaces of the CNTs completely, so that the measured specific surface areas should be smaller than the true values. The structures of the pristine CNT film and the CNT aerogel were also characterized by Raman spectroscopy. Raman spectra in Figure 4c consist of characteristic D band at about 1347 $cm^{-1}$ and G band at about 1580 $cm^{-1}$. The D band was usually attributed to the presence of surface defects of CNTs. The G band originated from in-plane vibrations of carbon atoms. Defect concentration in CNTs can be estimated by the ratio of intensities of D band and G band ($I_D/I_G$). CNT film showed an $I_D/I_G$ ratio of 1.12. The $I_D/I_G$ ratio increased to 1.31 for the CNT aerogel after immersion into the piranha solution, indicating the increase of the defect concentration of CNT aerogel. X-ray photoelectron spectroscopy (XPS) was also carried out to characterize the defect condition. The intensity of the O1s peak of the CNT aerogel was much higher compared to that for the CNT film (Figure 4d), indicating an increased amount of oxygen in the CNT aerogel, owing to the treatment with the piranha solution during the self-expansion process. C1s spectra of the CNT film can be deconvoluted into peaks corresponding to C=C and C−O bonds (Figure 4e). In addition to these peaks, deconvolution of the C1s XPS of the CNT aerogel illustrates the absorbance peaks of oxygen functionalities at 287.1 and 288.2 eV that can be attributed to −C=O− and −COO− species, respectively. Both Raman and XPS spectra suggest that the defect concentration of CNTs increased after the piranha treatments.

### 2.3. Mechanism of the Self-Expansion Phenomenon

Based on the experimental observation of bubbles escaping from the CNT film during the swelling process and the morphology of the CNT aerogel, we proposed a self-expansion mechanism of the CNT film. As schematically shown in **Figure 5**, the adjacent sheets in the CNT film are pushed apart by gases (mainly $O_2$) produced from $H_2O_2$ in the piranha solution, leading to the inflation phenomenon from the tightly arranged CNT film into the loosely connected CNT aerogel. To study the reaction mechanism in this system, CNT films were also placed in a concentrated $H_2SO_4$ or $H_2O_2$ solution separately; the CNT films did not expand at all in either solution. The CNT film was immersed in the concentrated $H_2SO_4$ solution, which indicated the solution infiltration into the CNT film. No bubbles were observed and the CNT film became curled up with almost no volume change. In the $H_2O_2$ solution, the CNT film floated on the surface,

  

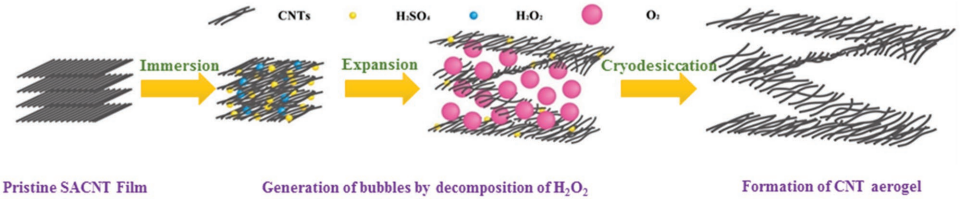


**Figure 5.** Schematic representation of the self-expansion mechanism of an SACNT film into a CNT aerogel.

which indicated that $H_2O_2$ could hardly permeate into the CNT film. As reported in the literature, $H_2O_2$ did not react with CNTs at room temperature.[23,32,33] Although bubbles were continuously produced in the $H_2O_2$ solution owing to the decomposition of $H_2O_2$ into $O_2$, these bubbles did not pass through the gaps between the CNT sheets in the film. Therefore, the CNT film did not expand in pure $H_2O_2$. The CNT film expanded spontaneously only in the piranha solution, which was a mixture of $H_2SO_4$ and $H_2O_2$. Therefore, the synergistic effect between $H_2SO_4$ and $H_2O_2$ contributed to the self-expansion of the CNT film. The wettability of the CNT film by $H_2SO_4$ and the decomposition of $H_2O_2$ into $O_2$ bubbles played equally vital roles. $H_2SO_4$ permeated into the gaps between the CNT sheets rapidly by capillary action and the oxidation process of the CNT film gradually occurred,[34] which could be evidenced by the XPS results (Figure 4e,f). The infiltration of $H_2O_2$ into the CNT film was greatly improved with the assistance of $H_2SO_4$. Figure S3 (Supporting Information) shows photographs of piranha solution droplets on a CNT film. Within 30 s, the wetting angle gradually reduced from 55° to 25°, demonstrating excellent wettability. Therefore, the piranha solution that entered the pores within the CNT aerogel could wet the CNT surface very well. Additionally, the decomposition of $H_2O_2$ was catalytically accelerated under acidic conditions. Therefore, $O_2$ was continuously generated at different positions in the gaps between the CNT sheets and extruded from the CNT film as large bubbles, leading to the self-expansion phenomenon of the CNT film.

The expansion rate of the CNT film was associated with the decomposition rate of $H_2O_2$. Figure S4 (Supporting Information) shows that the CNT film in piranha solution expanded at a faster rate at the beginning and then the expansion gradually slowed down during the first 5 h. During the expansion process, the amount of $H_2O_2$ was reduced and diluted over time, and the production rate of $O_2$ became slower. As a result, the expansion of the CNT film slowed down. The CNT film elongated ≈2.85 cm after immersion in piranha solution for 5 h. The elongated CNT film was immersed in new piranha solution for another 5 h, as indicated by the red arrow in Figure S4a (Supporting Information). The CNT film expanded quickly again with further elongation of 3.25 cm, similar to the elongation during the first 5 h. These results confirmed that the high concentration and large decomposition rate of $H_2O_2$ resulted in faster expansion of the CNT film. The volume ratio of the concentrated $H_2SO_4$ and $H_2O_2$ solution and layer number of the CNT film also affected the expansion rates of the aerogel. Figure S4b (Supporting Information) compares the variation of the length of the CNT aerogel in piranha solution with volume ratios of the concentrated $H_2SO_4$ and $H_2O_2$ solution at 9:1, 8:2, and 7:3. Higher content of $H_2O_2$ solution gave rise to faster aerogel expansion. Figure S4c (Supporting Information) demonstrates that the CNT film with 200 layers expanded faster than that with 100 layers. These results suggest that the expansion process of CNT aerogel can be accelerated by adding new piranha solution, using higher content of $H_2O_2$ solution and CNT film with more layers.

### 2.4. Application of Carbon-Coated CNT Aerogel in the Fields of Adsorption

Because of the high specific surface area and millimeter-sized macropores, the CNT aerogel was an ideal candidate for highly efficient solvent separation, such as adsorption of organic solvents and oils. To improve the mechanical properties and structural stability, the CNT aerogel was coated with a thin amorphous carbon layer by CVD before performing the adsorption experiments. In the literature, similar

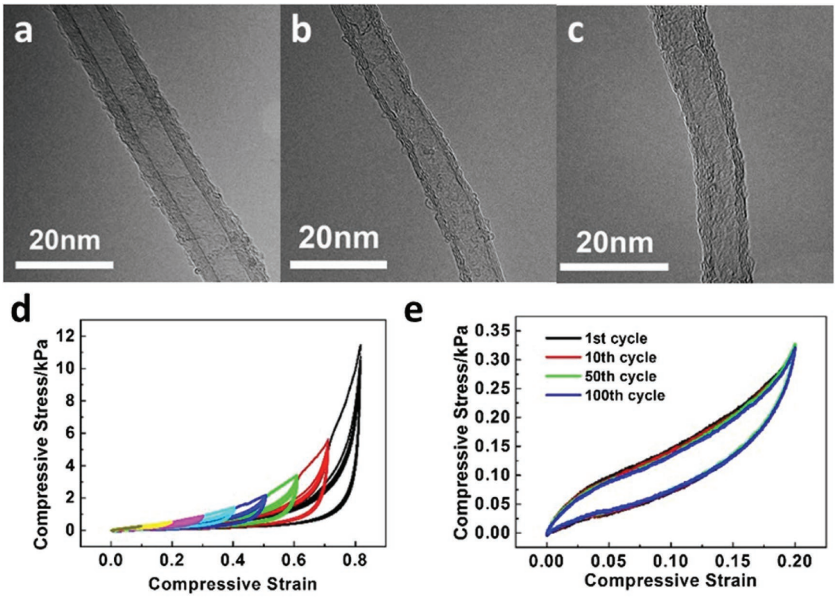


**Figure 6.** TEM images of a) pristine, b) CNT aerogel, and c) carbon-coated CNTs. Stress–strain curves of carbon-coated CNT aerogel ($\rho$ = 3 mg cm$^{-3}$) d) at different strains (10%–80%) and e) during 100 compressive cycles at 20% strain.

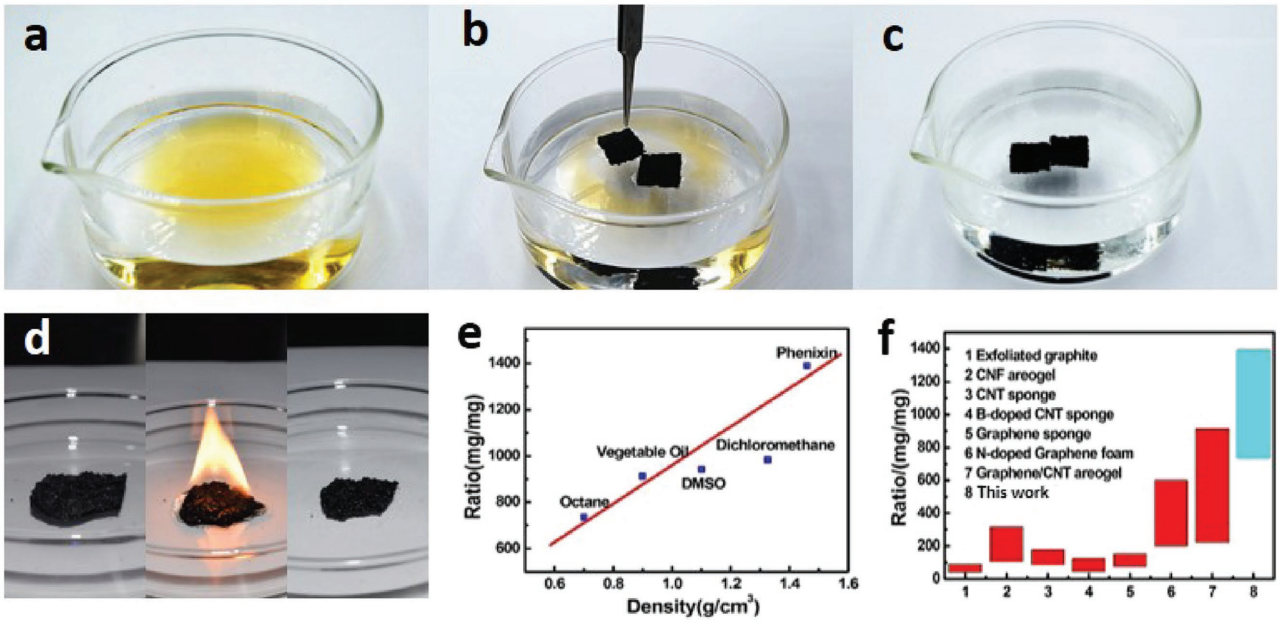


**Figure 7.** a–c) The adsorption of vegetable oil by the CNT aerogels. d) CNT aerogels can repeatedly be used by burning of the vegetable oil. e) Adsorption capacities of the CNT aerogels for various organic solvents and oils. f) Comparison of the adsorption capacities of different carbon aerogels.

pyrolysis method was used to enhance the resilience of the CNT aerogel, where polyacrylonitrile was used as the precursors.[15] However, the microstructures of these two kinds of CNT aerogels were quite different. The microstructure of the CNT aerogel in the literature was "cotton-like," while the CNT aerogel in this work was similar to "honeycomb," which resulted in a very low density. As shown in Figure S5a (Supporting Information), the carbon-coated CNT aerogel kept the macroporous and interconnected cellular structure after the CVD process. The surface morphology changes of CNTs were investigated by transmission electron microscopy (TEM). The original CNTs contained eight co-axial walls with a diameter of 10 nm (**Figure 6**a). After immersion in the piranha solution, the outer surfaces of CNTs were corroded with remaining four co-axial walls and a diameter of 7 nm (Figure 6b). The modification of CNTs by the piranha solution resulted in increased specific surface area of the CNT aerogel (298 $m^2$ $g^{-1}$) compared to the original CNT film (180 $m^2$ $g^{-1}$), as shown in the isothermal adsorption–desorption curves of the CNT aerogels (Figure S5b, Supporting Information). After the CVD process, the thickness of the carbon coating layer on CNT was ≈1 nm (Figure 6c). The specific surface area of the CNT aerogel after carbon coating reduced to 169 $m^2$ $g^{-1}$, indicating coverage of the surface defects by the amorphous carbon coating layer covered. The pore volume of the CNT aerogel remained almost unchanged before and after the carbon coating process. The mechanical properties of the CNT aerogel and the carbon-coated aerogel were also characterized by compressive tests. Figure 6d shows the compressive stress–strain curves of carbon-coated CNT aerogel that underwent five cycles at 80% strain, demonstrating outstanding elastic resilience and full recovery. Even after 100 compressive cycles at 20% strain, the shape of the carbon-coated CNT aerogel remained unchanged (Figure 6e). As shown in Figure S5c (Supporting Information), after the carbon coating, the compressive stress of the CNT aerogel significantly increased by four times and the Young's modulus increased from 2.11 to 3.44 kPa at 80% strain. After compression at nearly 100% strain and release, the pristine CNT aerogel permanently collapsed, while the carbon-coated CNT aerogel completely recovered to its original height (Figure S6, Supporting Information).

As shown in **Figure 7**a–c, two pieces of the carbon-coated CNT aerogels were used to adsorb oil floating on water. The oil was immediately adsorbed once it made contact with the CNT aerogels. The adsorbed oil could be burned off by setting fire to the carbon-coated CNT aerogel, and the carbon-coated CNT aerogel did not experience any irreversible shape distortion or weight loss. This feature could be attributed to the chemical stability and excellent mechanical strength of the carbon-coated CNT aerogel, and indicates that the carbon-coated CNT aerogel could be used repeatedly (Figure 7d). The adsorption capacity (the ratio of the weight of the CNT aerogel to the initial weight) of the original CNT aerogel to the vegetable oils was 400 mg $mg^{-1}$, and the adsorption capacity of the carbon-coated CNT aerogel to the vegetable oils increased to 912 mg $mg^{-1}$. The different adsorption capacity between pristine aerogel and carbon-coated CNT aerogel mainly arose from their different structural stability. The microstructure of the pristine CNT aerogel was unstable. After adsorbing the oils, the macroporous and interconnected cellular structure partly collapsed, thus limiting its adsorption capacity. In comparison, the carbon-coated CNT aerogel demonstrated excellent resilience, which was favorable for its structural stability and adsorption capacity. To investigate a wider range of potential applications, we

  

measured the adsorption of several other organic solvents using carbon-coated CNT aerogels with density of 0.5 mg $cm^{-3}$. The adsorption capacities of the carbon-coated CNT aerogel showed an approximately linear relationship with the densities of the organic solvents (Figure 7e), which mainly resulted from the fixed macropore volume in the carbon-coated CNT aerogel. The adsorption capacities for 1-octane, dimethyl sulfoxide, dichloromethane, and phenixin were 734, 940, 982, and 1389 mg $mg^{-1}$, respectively. Notably, the adsorption capacity for phenixin was almost two times higher than the highest values reported in the literature.[14,16,20,35–39] The adsorption capacities of the carbon-coated CNT aerogels were compared with different types of carbon aerogels reported in previous works, such as exfoliated graphite,[39] CNT fibers,[20,35] CNT sponges,[16,36] graphene aerogels,[37,38] and their composites[14] (Figure 7f). Among them, the carbon-coated CNT aerogel in this work demonstrated the highest physical adsorption capacity, which was attributed to the ultrahigh porosity, high specific surface area, extremely low density, and excellent mechanical properties of the carbon-coated CNT aerogel. All the CNT bundles were well dispersed and interwoven into the cell walls in the carbon-coated CNT aerogel. The capillary action within the carbon-coated CNT aerogel helped to adsorb the organic solvent effectively, which was then constrained inside the cells encircled by strong CNT sheets.

## 3. Conclusion

We developed a novel and simple strategy for scalable fabrication of macroscopic, ultralight, and 3D pure CNT aerogels through the self-expansion of SACNT films. The CNT aerogels exhibited a typical hierarchical porous and cellular structure, which was assembled from giant and ultrathin SACNT sheets as cell walls. The aerogels were ultralight (0.12 mg $cm^{-3}$), hydrophobic, chemically stable, and had an ultrahigh porosity (>99.95%) and a high specific surface area (298 $m^2$ $g^{-1}$). The densities and shapes of the CNT aerogels could be controlled. The CNT aerogel showed high adsorption capacities of various kinds of organic solvents and oils. In addition, the ultralight and macroporous CNT aerogels also hold potential for a wide range of applications, such as energy storage, catalysis, and bioengineering.

## 4. Experimental Section

*Preparation of SACNT Film and CNT Aerogel*: The procedure for the synthesis of SACNTs was reported in previous studies.[6] SACNT film was drawn from an SACNT array on a 4 inch silicon wafer, then collected onto a roller and cut into 3 × 3 $cm^2$ pieces. The piranha solution was prepared by mixing 98 wt% concentrated $H_2SO_4$ and 35 wt% $H_2O_2$ in a quartz sink at a volume ratio of 7:3. A CNT film was placed in the piranha solution and expanded spontaneously into a CNT aerogel. After a few days, the CNT aerogel was repeatedly rinsed with deionized water until the pH value reached 7. The CNT aerogel was then transferred into a beaker or a petri dish for the following freeze-drying process using freeze drying equipment (Four-Ring, LGD-10D).

*Characterization of SACNT Film and CNT Aerogel*: The morphology and structure of the SACNT film and CNT aerogel were characterized using an optical microscope (ZEISS KL1500 LCD), a scanning electron microscope (SEM, FEI Sirion 200) operating at 10 kV and FEI Tecnai G2F20 transmission electron microscope (TEM) operating at 200 kV. The orientation and alignment of the SACNT films and CNT aerogels were determined using pole figure (0° < chi < 90°, 0° < phi < 360°) measurements of X-ray diffraction (Rigaku Smartlab) by recording the (002) diffraction peak ($2\theta$ = 26°). BET and Barrett–Joyner–Halenda measurements were performed on a surface area and porosity analyzer (ASAP 2020). XPS analysis was performed on a PHI5300 spectrometer. Raman spectra of CNT film and CNT aerogel after immersion into piranha solution were recorded on a Horiba spectrometer. Compressive tests were performed using an Instron 5848 microtester at a strain rate of 5 mm $min^{-1}$ and the dimensions of the samples were 1 cm × 1 cm × 1 cm.

## Supporting Information

*Supporting Information is available from the Wiley Online Library or from the author.*

## Acknowledgements

*Y.F.L. and S.L. contributed equally to this work. This work was supported by the NSFC (51472141) and National Basic Research Program of China (2012CB932301).*

## Conflict of Interest

*The authors declare no conflict of interest.*

[1] S. Iijima, *Nature* **1991**, *354*, 56.
[2] R. F. Zhang, Y. Y. Zhang, Q. Zhang, H. H. Xie, W. Z. Qian, F. Wei, *ACS Nano* **2013**, *7*, 6156.
[3] H. M. Wei, Y. Wei, Y. Wu, L. Liu, S. S. Fan, K. L. Jiang, *Nano Res.* **2013**, *6*, 208.
[4] M. Endo, H. Muramatsa, T. Hayashi, Y. A. Kim, M. Terrones, M. S. Dresselhaus, *Nature* **2005**, *433*, 476.
[5] A. Y. Cao, P. L. Dickrell, W. G. Sawyer, M. N. Ghasemi-Nejhad, P. M. Ajayan, *Science* **2005**, *310*, 1307.
[6] M. B. Bryning, D. E. Milkie, M. F. Islam, L. A. Hough, J. M. Kikkawa, A. G. Yodh, *Adv. Mater.* **2007**, *19*, 661.
[7] K. H. Kim, Y. Oh, M. F. Islam, *Adv. Funct. Mater.* **2013**, *23*, 377.
[8] Y. Wu, Y. Wei, J. P. Wang, K. L. Jiang, S. S. Fan, *Nano Lett.* **2013**, *13*, 818.
[9] A. L. M. Reddy, M. M. Shaijumon, S. R. Gowda, P. M. Ajayan, *Nano Lett.* **2009**, *9*, 1002.
[10] H. B. Li, X. C. Gui, L. H. Zhang, S. S. Wang, C. Y. Ji, J. Q. Wei, K. L. Wang, H. W. Zhu, D. H. Wu, A. Y. Cao, *Chem. Commun.* **2010**, *46*, 7966.

  

[11] Y. Yang, Y. H. Deng, Z. Tong, C. Y. Wang, *J. Mater. Chem. A* **2014**, *2*, 9994.
[12] A. E. Aliev, J. Oh, M. E. Kozlov, A. A. Kuznetsov, S. L. Fang, A. F. Fonseca, R. Ovalle, M. D. Lima, M. H. Haque, Y. N. Gartstein, M. Zhang, A. A. Zakhidov, R. H. Baughman, *Science* **2009**, *323*, 1575.
[13] B. Wicklein, A. Kocjan, G. S. Alvarez, F. Carosio, G. Camino, M. Antonietti, L. Bergstrom, *Nat. Nanotechnol.* **2015**, *10*, 277.
[14] H. Y. Sun, Z. Xu, C. Gao, *Adv. Mater.* **2013**, *25*, 2554.
[15] K. H. Kim, Y. Oh, M. F. Islam, *Nat. Nanotechnol.* **2012**, *7*, 562.
[16] X. C. Gui, J. Q. Wei, K. L. Wang, A. Y. Cao, H. W. Zhu, Y. Jia, Q. K. Shu, D. H. Wu, *Adv. Mater.* **2010**, *22*, 617.
[17] W. Q. Zhao, Y. B. Li, S. S. Wang, X. D. He, Y. Y. Shang, Q. Y. Peng, C. Wang, S. Y. Du, X. C. Gui, Y. B. Yang, Q. Yuan, E. Z. Shi, S. T. Wu, W. J. Xu, A. Y. Cao, *Carbon* **2014**, *76*, 19.
[18] M. Zhang, S. Fang, A. A. Zakhidov, S. B. Lee, A. E. Aliev, C. D. Williams, K. R. Atkinson, R. H. Baughman, *Science* **2005**, *309*, 1215.
[19] J. H. Zou, J. H. Liu, A. S. Karakoti, A. Kumar, D. Joung, Q. Li, S. I. Khondaker, S. Seal, L. Zhai, *ACS Nano* **2010**, *4*, 7293.
[20] Z. Y. Wu, C. Li, H. W. Liang, J. F. Chen, S. H. Yu, *Angew. Chem. Int. Ed.* **2013**, *52*, 2925.
[21] K. L. Jiang, Q. Q. Li, S. S. Fan, *Nature* **2002**, *419*, 801.
[22] X. B. Zhang, K. L. Jiang, C. Feng, P. Liu, L. N. Zhang, J. Kong, T. H. Zhang, Q. Q. Li, S. S. Fan, *Adv. Mater.* **2006**, *18*, 1505.
[23] K. L. Jiang, J.P. Wang, Q. Q. Li, L. Liu, C. H. Liu, S. S. Fan, *Adv. Mater.* **2011**, *23*, 1154.
[24] M. Y. Li, Y. Wu, F. Zhao, Y. Wei, J. P. Wang, K. L. Jiang, S. S. Fan, *Carbon* **2014**, *69*, 444.
[25] Y. Koo, V. N. Shanov, S. Yarmolenko, M. Schulz, J. Sankar, Y. Yun, *Langmuir* **2015**, *31*, 7616.
[26] Y. F. Liu, L. D. Nguyen, T. T. Huu, Y. Liu, T. Romero, L. Janowska, D. Begin, C. P. Huu, *Mater. Lett.* **2012**, *79*, 128.
[27] S. H. Zeng, L. Zhang, N. Jiang, M. Y. Gao, X. Z. Zhao, Y. L. Yin, H. Q. Su, *J. Power Sources* **2015**, *293*, 1016.
[28] J. J. Yu, W. Du, F. Q. Zhao, B. Z. Zeng, *Electrochim. Acta* **2009**, 984.
[29] R. Smajda, A. Kukovecz, Z. Konya, I. Kiricsi, *Carbon* **2007**, 1176.
[30] A. Peigney, Ch. Laurent, E. Flahaut, R. R. Bacsa, A. Rousset, *Carbon* **2001**, *39*, 507.
[31] R. Raccichini, A. Varzi, S. Passerini, B. Scrosatl, *Nat. Mater.* **2015**, *14*, 271.
[32] K. A. Wepansnick, B. A. Smith, K. E. Schrote, H. K. Wilson, S. R. Diegelmann, D. H. Fairbrother, *Carbon* **2011**, *49*, 24.
[33] S. H. Liu, J. R. Wu, *Int. J. Hydrogen Energy* **2012**, *37*, 16994.
[34] F. Y. Kang, Y. Leng, T. Y. Zhang, *J. Phys. Chem. Solids* **1996**, *57*, 889.
[35] S. D. Yang, L. Chen, L. Mu, B. Hao, P. C. Ma, *RSC Adv.* **2015**, *5*, 38470.
[36] D. P. Hashim, N. T. Narayanan, J. M. R. Herrera, D. A. Cullen, M. G. Hahm, P. Lezzi, J. R. Suttle, D. Kelkhoff, E. M. Sandoval, S. Ganguli, A. K. Roy, D. J. Smith, R. Vajtai, B. G. Sumpter, V. Meunier, H. Terrones, M. Terrones, P. M. Ajayan, *Sci. Rep.* **2012**, *2*, 363.
[37] J. P. Zhao, W. C. Ren, H. M. Chen, *J. Mater. Chem.* **2012**, *22*, 20197.
[38] Y. Zhao, C. G. Hu, Y. Hu, H. H. Cheng, G. Q. Shi, L. T. Qu, *Angew. Chem. Int. Ed.* **2012**, *51*, 11371.
[39] M. Toyoda, M. Inagaki, *Carbon* **2000**, *38*, 199.

Received: March 24, 2017
Published online: May 26, 2017

  